ORGANOMETALLICS

Article

Cite This: *Organometallics* XXXX, XXX, XXX−XXX

(Pyridin-2-yl)-NHC Organoruthenium Complexes: Antiproliferative Properties and Reactivity toward Biomolecules

Sanam Movassaghi,[†] Sukhjit Singh,[†] Aewan Mansur,[†] Kelvin K. H. Tong,[†] Muhammad Hanif,[†] Hannah U. Holtkamp,[†] Tilo Söhnel,[†] Stephen M. F. Jamieson,[‡] and Christian G. Hartinger*[,†]

[†]School of Chemical Sciences, University of Auckland, Private Bag 92019, Auckland 1142, New Zealand

[‡]Auckland Cancer Society Research Centre, University of Auckland, Private Bag 92019, Auckland 1142, New Zealand

Supporting Information

ABSTRACT: Organoruthenium compounds have been widely investigated for their anticancer activity. Here we use one of the classic ligand classes found in organometallics, i.e., N-heterocyclic carbenes (NHC), and coordinate them to the Ru(η^6-*p*-cymene) scaffold as *N*,*C*-bidentate ligands substituted with a pyridyl moiety. Introduction of different substituents gave compounds with a wide variety of properties. We investigated their stability in solution and in the presence of biomolecules, in vitro anticancer activity, and cellular uptake to rationalize their biological properties in dependence on the structure. A clear effect of their structure on the stability in water and DMSO was found for some derivatives, which was reflected in the reactivity to biomolecules that was determined with selected representatives of the compound classes. The antiproliferative activity of the compounds was widely dependent on the lipophilicity of the *N*,*C*-bidentate ligand, but as cellular accumulation studies revealed, lipophilicity does not provide the full picture and additional effects must be responsible for the anticancer activity.

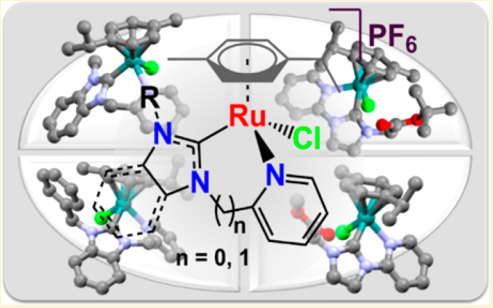

INTRODUCTION

N-Heterocyclic carbenes (NHC) are currently receiving much attention for their wide application in coordination chemistry and catalysis.[1,2] In the latter area, NHC ligands are considered an alternative to phosphanes,[1−5] and a large number of different monodentate NHC ligands derived from imidazole, imidazolidine, benzimidazole, and triazole[6] have been synthesized.[6,7] They have been used in a number of chemical transformations,[8] including palladium-catalyzed C−N coupling reactions,[9,10] rhodium-catalyzed hydroformylation,[11] ruthenium-catalyzed olefin metathesis reactions,[12] and Heck- and Suzuki-type C−C coupling reactions.[13] NHCs can also be part of larger, multidentate ligand systems, such as in combination with pyridyl groups, where for example a tridentate pincer framework gave remarkable catalytic activities in the Heck reaction.[1,8,14,15]

More recently, NHC ligands have entered the area of medicinal inorganic chemistry.[16−19] For example, metal−NHC complexes (Figure 1) have been investigated for the treatment of cancer and infectious diseases. The earliest documentation of metal−NHC complexes with promise for medicinal applications was on Ru^{II} and Rh^{I} organometallics which expressed antibacterial properties.[19−22] Later, Youngs and co-workers reported Ag−NHC compounds with outstanding antimicrobial activity against both Gram-positive and/or Gram-negative bacteria.[23] The effective antimicrobial properties of the Ag−NHC complexes were concluded to be a result of the slow release of Ag^+ ions from the stabilizing ligands into the culture medium.[23] Inspired by the use of gold(I) complexes in the therapy of rheumatoid arthritis, researchers reported a series of NHC−Au^{I} complexes derived from imidazolium salts as anticancer agents.[16,24] The lipophilicity of linear Au^{I} complexes led to the triggering of Ca^{2+}-sensitive mitochondrial swelling.[25] The primary mode of action for the NHC−Au^{I} complexes is thought to involve targeting the enzyme thioredoxin reductase (TrxR),[26] which plays an important role in sustaining the intracellular redox homeostasis, promotes cell growth and survival, and is upregulated in some cancer types.[24,26]

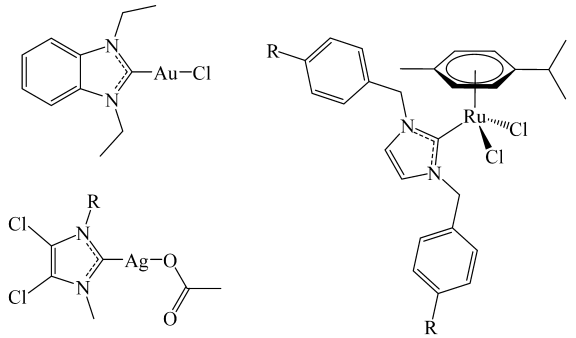

Figure 1. Exemplary structures for metal−NHC complexes with promising properties for medicinal applications.

Ru^{II}(arene) complexes of the general formula [Ru^{II}(arene)(X)(Y)(Z)] are well-established bioactive compounds.[27−31] The ligands coordinated to the Ru center can be mono- or

Received: March 12, 2018

DOI: 10.1021/acs.organomet.8b00153
Organometallics XXXX, XXX, XXX−XXX

Scheme 1. Preparation of the Ru Complexes 1a−10a[a]

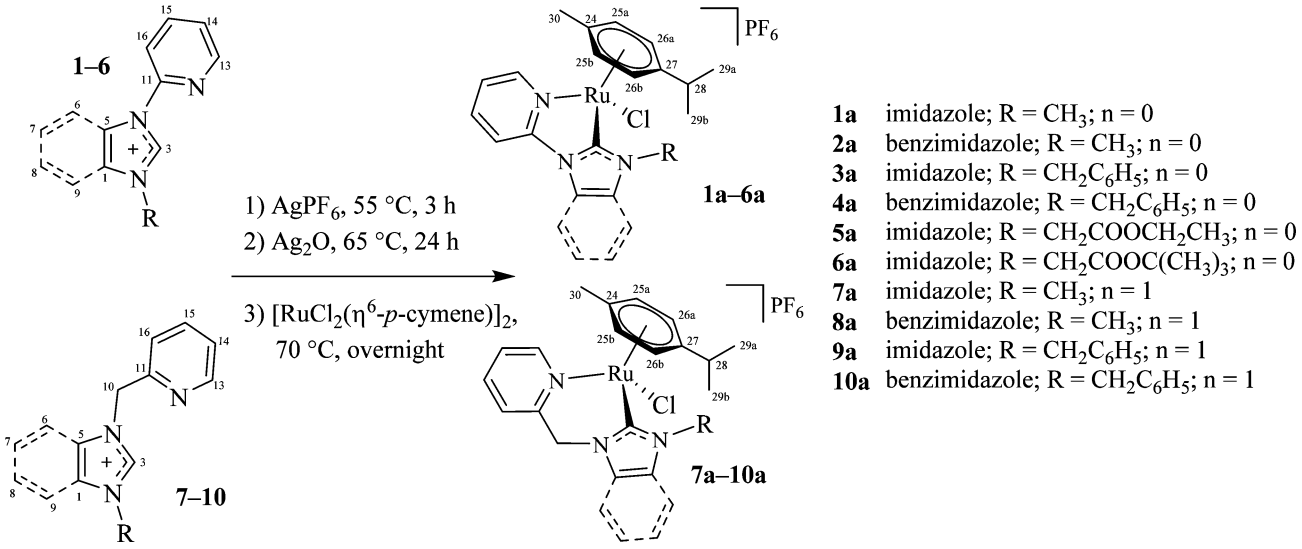

1a imidazole; R = CH_3; n = 0
2a benzimidazole; R = CH_3; n = 0
3a imidazole; R = $CH_2C_6H_5$; n = 0
4a benzimidazole; R = $CH_2C_6H_5$; n = 0
5a imidazole; R = $CH_2COOCH_2CH_3$; n = 0
6a imidazole; R = $CH_2COOC(CH_3)_3$; n = 0
7a imidazole; R = CH_3; n = 1
8a benzimidazole; R = CH_3; n = 1
9a imidazole; R = $CH_2C_6H_5$; n = 1
10a benzimidazole; R = $CH_2C_6H_5$; n = 1

[a]The counterions to the imidazolium compounds **1**−**10** were bromide (**3**−**5**, **7**, **9**, **10**) or iodide (**1**, **2**, **8**). The numbering scheme was used to assign the peaks observed in the NMR spectra.

multidentate and influence the chemical and biological properties of the compounds.[32−37] NHC ligands coordinated to bioactive metals such as Ru afforded remarkably stable complexes and some (benz)imidazole-derived NHC−Ru complexes exhibited strong antiproliferative effects possibly through inhibition of TrxR.[38] In comparison to the number of monodentate NHC ligands used in complexes with biological properties, the literature is scarce for bioactive complexes that feature bidentate ligands containing an NHC group.[16,19] In this paper, we aim to fill this gap with the introduction of *N*,*C*-coordinating pyridyl-functionalized NHC ligands and studies on the effect of such modifications on stability and reactivity toward biomolecules as well as in vitro cytotoxicity and cellular uptake.

RESULTS AND DISCUSSION

The precursors 2-(1*H*-imidazol-1-yl)pyridine (**I**), 2-(1*H*-benzimidazol-1-yl)pyridine (**II**), 1-(2-pyridinylmethyl)-1*H*-imidazole (**III**), and 1-(2-pyridinylmethyl)-1*H*-benzimidazole (**IV**) were prepared using a modified Ullman-type Cu^I coupling reaction between 2-bromopyridine derivatives and the chosen azole in DMSO instead of DMF and by replacement of K_2CO_3 with K_3PO_4.[39−43] The subsequent *N*-alkylation of the second imidazole nitrogen atom in **I**−**IV** afforded **1**−**10** in mostly high yields (Table S1), following literature procedures for **1**−**5** and **7**−**10**.[39−43] The identity of precursors **I**−**IV** and ligands **1**−**10** was confirmed by NMR spectroscopy and electrospray ionization mass spectrometry (ESI-MS; Table S2 in the Supporting Information). In the case of the ethyl ester derivative **5**, the ESI mass spectra showed a transesterification with methanol during the analysis of the compounds.

The synthesis of the Ru^{II}(arene) compounds was initially attempted using the classic silver-mediated transmetalation with Ag_2O to form an Ag(NHC) intermediate, to which $[Ru^{II}(\eta^6\text{-}p\text{-cymene})Cl_2]_2$ was added.[44−46] However, this strategy was unsuccessful and instead a route starting with first $AgPF_6$ and subsequently adding Ag_2O and $[Ru^{II}(\eta^6\text{-}p\text{-cymene})X_2]_2$ was used (Scheme 1). The presence of the halide in the complexation reaction led to the formation of an insoluble product and caused difficulties in the isolation of the products, and addition of $AgPF_6$ to the imidazolium halides leads to the formation of AgX (X = Br, I).[41] A solvent combination of dichloromethane (DCM) and 1,2-dichloroethane (DCE) (3/1) provided the best results to afford the bidentate NHC complexes. The imidazolium carbene precursor was dissolved in DCE before DCM was added. Addition of $AgPF_6$ to the mixture caused immediate precipitation of AgX, indicating halide/PF_6 metathesis. The reaction mixture was then kept in darkness and stirred at 55 °C for 3 h before Ag_2O was added, and the temperature was increased to 65 °C to produce the Ag^I(NHC-pyridin-2-yl) intermediate. A reaction time of 24 h was identified as the optimal time to allow for complete conversion. Then, $[Ru^{II}(\eta^6\text{-}p\text{-cymene})X_2]_2$ was added and the reaction mixture was stirred overnight. The stoichiometry of Ag_2O and NHC-pyridin-2-yl precursor was identified as crucial for successful conversion, and the highest yield and purity were obtained when ratios of around 2:2.5:1.5:1.5 of NHC precursor, $AgPF_6$, Ag_2O, and $[RuCl_2(\eta^6\text{-}p\text{-cymene})]_2$ were used (see the Experimental Section for the exact ratios used for the individual complexes). This synthetic approach allowed the isolation of the novel compounds **4a**−**6a**, **9a**, and **10a**, while **1a**−**3a**, **7a**, and **8a** have been reported earlier.[15,47−49]

Characterization of the complexes by NMR, ESI-MS, elemental analysis, and X-ray diffraction (for the new derivatives **4a**−**6a** and **10a**) indicated successful formation of **1a**−**10a**, in which the ligands can form five- or six-membered rings with the Ru center. In the ^{1}H NMR spectra, the absence of a signal assignable to the pro-carbenic proton H-3 (see Scheme 1 for the atom labeling) and the downfield shift (from 8.7 to 9.4 ppm) of H-13 suggested that the Ru^{II} center coordinated to the bidentate ligand through its C-3 and N-12 atoms. Introduction of the $Ru^{II}(\eta^6\text{-}p\text{-cymene})$ moiety resulted in several distinct signals in the aromatic and aliphatic regions. In addition, the protons of the methylene linker between the (benz)imidazole and/or of the CH_2 group of the benzyl or of the 2-acetyl substituents became diastereotopic upon metal coordination (see Figure S1). The *p*-cymene aromatic protons H-25a/b and H-26a/b were observed in the range of 5.76−6.45 ppm as four individual doublets, which is common for compounds featuring bidentate coligands.

DOI: 10.1021/acs.organomet.8b00153
Organometallics XXXX, XXX, XXX−XXX

Table 1. Key Bond Lengths (Å) and Angles (deg) for 4a, 5a, 7a, 10a, and 12a

	4a	5a	6a	8a[a]	10a
			Bond Length/Å		
Ru−Cl	2.4012(6)	2.3999(6)	2.4152(5)	2.395(3), 2.404(3)	2.414(1)
Ru−C_{NHC}	1.997(2)	2.017(3)	2.012(2)	2.022(9), 2.013(9)	2.039(6)
Ru−N_{Py}	2.080(2)	2.100(2)	2.1079(17)	2.133(8), 2.134(7)	2.114(2)
			Bond Angle/deg		
C_{NHC}−Ru−N_{Py}	76.09(10)	76.28(10)	76.44(7)	84.7(4), 85.1(3)	85.31
Cl−Ru−N_{Py}	85.73(6)	86.52(6)	87.60(5)	86.3(3), 86.5(3)	84.69
Cl−Ru−C_{NHC}	84.20(8)	83.00(8)	82.87(6)	86.5(3), 87.7(3)	87.80

[a]Two crystallographically independent molecules.

The NMR data were supported by ESI-MS studies, providing further confirmation of the identity of the complexes synthesized. The ESI-mass spectra contained mainly the pseudomolecular ions $[M - PF_6]^+$ (Table S3). In addition, for **5a** transesterification to the methyl ester was detected, most probably again due to MeOH being used as the solvent for the MS experiments. The compounds were found to be hygroscopic, and the elemental analyses indicated for several compounds the presence of solvent molecules. Furthermore, the X-ray crystallographic data for **4a** indicated the presence of small amounts of bromido instead of chlorido ligands (see below).

Single crystals suitable for X-ray diffraction analysis of **4a**−**6a**, **8a**, and **10a** were grown via slow diffusion of diethyl ether into a saturated solution of the complex in acetone. The X-ray crystallographic data for all complexes are given in Table S4 and the key bond parameters in Table 1. Complexes **5a** and **6a** crystallized in the triclinic space group $P\bar{1}$, while **4a**, **8a**, and **10a** crystallized in the monoclinic, orthorhombic, and monoclinic space groups $P2_1/n$, $Pna2_1$, and $I2/c$, respectively. As expected, the complexes adopted a pseudo-octahedral piano-stool configuration (Figure 2 and Figure S2), with the *p*-cymene acting as the seat and the bidentate NHC ligand and chlorido group as the legs. In all cases the complexes crystallized as a mixture of enantiomers with the chiral center located at the metal. The structures of **8a** and **10a** feature a methylene spacer between the NHC and the pyridyl groups, which is absent in **4a**−**6a**. Therefore, the latter structures form a virtually planar five-membered ring with the ruthenium center. In the structures of **8a** and **10a**, the metal center is part of a six-membered ring system and the planarity is absent. This makes the latter compounds less rigid.

For complex **4a** the Ru−C_{NHC} bond length is the shortest of the structures analyzed (1.997(3) Å), while **10a** features the longest bond (2.039(6) Å). The Ru−Cl bonds were, as expected, in the range of 2.4 Å. Note that the structure of **4a** was refined with 11.4(3)% Br replacing the chlorido ligands. The Ru−N bond in **8a** is notably longer than in the other complexes (Table 1). Inspection of the structures of **8a** and **10a** revealed that the methylene protons are in different chemical environments, explaining the diastereotopic behavior in the ^{1}H NMR spectroscopy experiments. For complexes **4a**, **8a**, and **10a** π-stacking interactions were observed to occur between the benzimidazole moieties of the NHC ligands of the two enantiomers found in the molecular structures (Figure S3 for **4a**). In contrast, in the structures of **5a** and **6a** (Figure S2), the π-stacking interactions were formed between the pyridyl rings of the two enantiomers. The shortest distances were found for **4a** at 3.357 Å, followed by **10a** (3.376 Å), **6a** (3.378 Å), **8a** (3.473 Å), and **5a** (3.510 Å). Notably, for **5a** a mixture of the methyl and ethyl derivatives (36(1):64(1)) was identified in the single crystal, confirming the propensity of transesterification of the compound class.

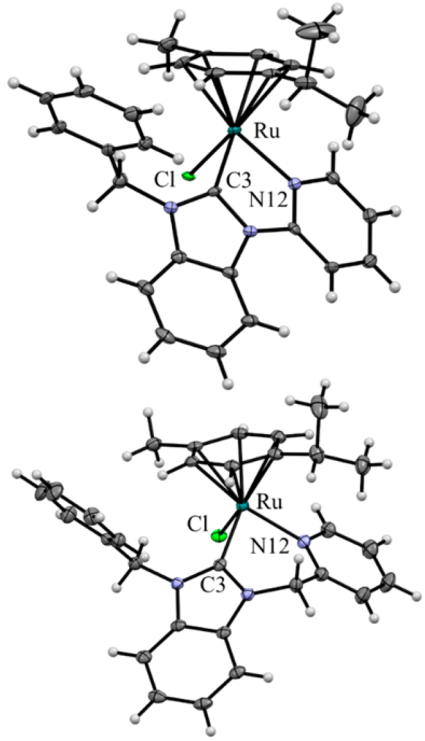

Figure 2. ORTEP representations of the molecular structure of one of the enantiomers of **4a** (top) and of **10a** (bottom) drawn at 50% probability ellipsoid levels. The counterions and any solvent molecules were omitted for clarity.

Stability in DMSO and Aqueous Solution. Representative examples of complexes where the Ru center is part of five (**1a**−**3a**)- or six-membered (**8a** and **10a**) rings as well as **5a** and **6a** bearing an ester moiety were selected for stability studies in DMSO-d_6 and/or 20% DMSO-d_6/80% D_2O by ^{1}H NMR spectroscopy (Table S5). In general, the compounds were fairly stable in DMSO-d_6; however, over time a slow release of the *p*-cymene ligand was observed, as indicated by the appearance of signals at around 7 ppm in the ^{1}H NMR spectra (compare Figure 3 for **1a**). Compound **1a** was the least stable of the complexes investigated in terms of *p*-cymene release, while bulkier groups around the metal center were found to give higher stability. The presence of the methylene linker did not influence the stability in DMSO significantly (compare Figure S4 for **8a**). In the case of the ester derivatives **5a** and **6a**, minor arene ligand cleavage was observed. It appears that the ethyl ester moiety of **5a** reacted slowly with residual water in the NMR solvent, yielding a carboxylic acid, while **6a** did not seem to undergo such a hydrolysis process. The ^{1}H NMR spectra of **5a** featured increasing signals at about 1.1 ppm which can be

DOI: 10.1021/acs.organomet.8b00153
Organometallics XXXX, XXX, XXX−XXX

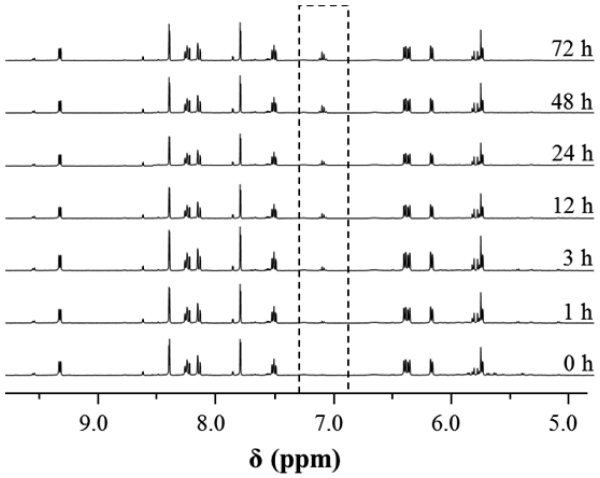

Figure 3. Time-dependent ^{1}H NMR spectroscopic stability study for **1a** in DMSO-d_6 over 72 h. The box denotes peaks assigned to the slow release of the *p*-cymene ligand.

assigned to the CH_3 group of ethanol (Figure S5), while the signal of the CH_2 group was covered by the water peak.

For the investigation of aqueous stability, studies were conducted for **2a** and **8a**, which were dissolved in DMSO-d_6, followed by immediate dilution with D_2O to give a DMSO-d_6:D_2O ratio of 1:5 and analysis by ^{1}H NMR spectroscopy. Compound **8a** was very stable with no signs of chlorido/aqua ligand exchange observed, even after 72 h of incubation at room temperature (Figure S6). In contrast, **2a** underwent a ligand exchange reaction to form the respective aqua complex $\mathbf{2a}^{H2O}$ with the first signs of a second species appearing in the ^{1}H NMR spectrum recorded after about 12 h of dissolution. The formation of the aqua complex was indicated by additional peaks appearing in both the aromatic and aliphatic regions of the ^{1}H NMR spectra. Very notable changes were observed for H-13, which shifted upfield to about 9.2 ppm. Furthermore, the *p*-cymene protons were detected downfield of those assigned to the chlorido complex (Figure 4). The assignment of these peaks as the respective aqua species was achieved by experiments in which $AgNO_3$ was added to the reaction mixture (Figure S7), and comparison of the ^{1}H NMR spectra showed large overlaps with the signals obtained in DMSO-d_6/D_2O (Figure 4). In addition, *p*-cymene cleavage was observed to occur after around 1 day of dissolution (gray shaded box in Figure 4). Similar observations were made in the reaction of **5a** with $AgNO_3$ in DMSO-d_6/D_2O, while **8a** could not be activated under these conditions (data not shown). This behavior for **8a** also confirms the observations made in pure DMSO-d_6.

In general it appears that complexes with ligands which form six-membered rings with the metal center are more stable than five-membered metallacycles, especially if they contain bulky groups on the NHC. However, the stability studies indicate that the compounds have sufficient stability for the preparation of samples for biological assays.

The exchange of the chlorido ligands of **1a** and **7a** was also investigated by density functional theory (DFT) calculations in water and the gas phase using GAUSSIAN 09W. In both cases the calculated energy difference for a Cl^-/H_2O ligand exchange was slightly positive (Table S6; ΔE_{1a} = 4.5 kcal/mol, ΔE_{7a} = 7.9 kcal/mol). However, the calculations suggest that the formation of hydroxido complexes is energetically favored (ΔE_{1a} = −59.5 kcal/mol, ΔE_{7a} = −66.0 kcal/mol). This may be related to the charge of the complex cation, which changes from

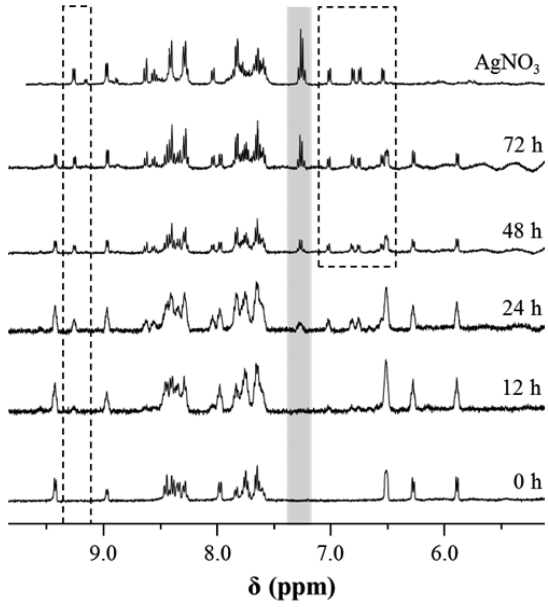

Figure 4. Time-dependent ^{1}H NMR spectroscopic stability study for **2a** in DMSO-d_6/D_2O over 72 h and for comparison a spectrum recorded 72 h after addition of $AgNO_3$. The gray shaded box denotes peaks assigned to the slow release of the *p*-cymene ligand. The boxes with the dashed lines indicate the peaks assigned to the aqua complex formed over time.

1+ to 2+ in case of Cl^-/H_2O exchange but remains constant for Cl^-/OH^-. Both complexes gave very similar results in these calculations, and the energetically favorable formation of hydroxido complexes will likely affect the pK_a values of their aqua complexes in solution. When the pH values of aqueous solutions of both **1a** and **7a** (0.7 μM) were measured, values of 4.9 and 4.2, respectively, were found. Analysis of the frontier molecular orbitals of $[\mathbf{1a}]^+$ and $[\mathbf{7a}]^+$ and their respective aqua and hydroxido analogues $[\mathbf{1a}/\mathbf{7a}^{H2O}]^{2+}$ and $[\mathbf{1a}/\mathbf{7a}^{OH}]^+$ (Figures S8 and S9) revealed that the LUMO orbitals of $[\mathbf{1a}]^+$ and its derivatives are delocalized over the metal center and ligands with the Ru *d* orbitals and π electrons of the pyridyl group contribute extensively, while the π electrons of the carbene moiety only partially contribute. The HOMOs of $[\mathbf{1a}]^+$ and $[\mathbf{1a}^{H2O}]^{2+}$ showed similar Ru *d* orbital contribution and involve π electrons of the imidazolium moiety rather than of the pyridyl group. The HOMOs of $[\mathbf{1a}^{OH}]^+$ are delocalized over the Ru center and the OH^- ligand. For $[\mathbf{7a}]^+$, the HOMO and LUMO orbitals are similar to each other, with the orbitals delocalized over the metal center and ligands. In contrast to the LUMOs of $[\mathbf{7a}]^+$ and its derivatives, the pyridyl group did not contribute to the LUMOs or HOMOs.

Interactions with Biological Molecules. Metallodrugs are exposed to a variety of biomolecules once administered to a living organism. Their pharmacological properties depend on the nature of these interactions. In order to investigate the NHC complexes for their reactivity with biomolecules, the five- and six-membered metallacycles **1a** and **7a** were selected for studies with the small biological molecules L-cysteine (Cys), L-methionine (Met), L-histidine, and 9-ethylguanine (EtG) in 10% D_6-DMSO/D_2O. The reactions were monitored by ^{1}H NMR spectroscopy for up to 2 days.

The reaction of **7a** with His at a molar ratio of 1:1 was monitored over a period of 24 h and resulted in the immediate formation of a dative bond between the imidazole-*N* and the ruthenium center by exchange of a chlorido ligand (Figure 5).

DOI: 10.1021/acs.organomet.8b00153
Organometallics XXXX, XXX, XXX−XXX

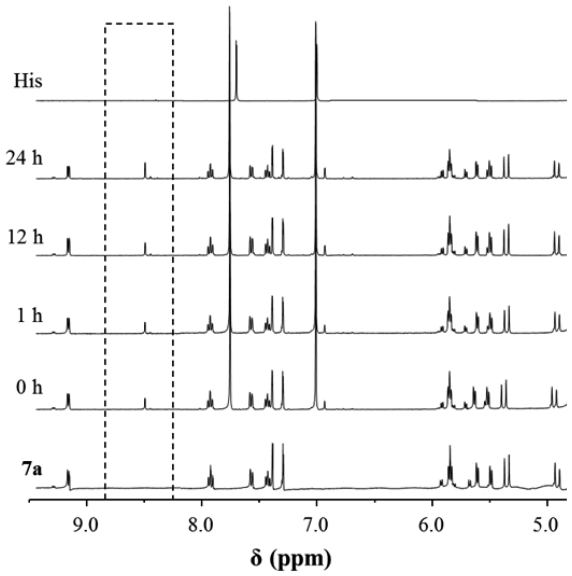

Figure 5. ^{1}H NMR spectroscopic study of the reaction between **7a** and His in 10% DMSO-d_6/D_2O, monitored for a period of 24 h. The new peaks assigned to the complex reacted with His are highlighted in a box.

This was indicated by the appearance of a new signal in the ^{1}H NMR spectra at about 8.5 ppm which was assigned to H-$2_{imidazole}$ of His. A significant downfield shift of about 0.8 ppm clearly indicates coordination of Ru to the *N*-imidazole moiety of His. The five-membered metallacycle **1a** also initially reacted with His in a similar fashion. However, over the course of the experiment, several sets of signals were detected in the ^{1}H NMR spectra, which may be a sign of further reactions taking place, possibly with His acting as a bidentate ligand (Figure S10). This clearly shows that there are differing degrees of reactivity between the two classes of compounds, with the six-membered metallacycle being more stable than the five-membered analogues.

Neither **1a** nor **7a** reacted with Cys (molar ratio of 1:1) to form defined products (Figures. S11 and S12). While **7a** was remarkably stable, given that many other Ru(arene) compounds decompose within minutes when reacted with Cys,[50−52] **1a** underwent slow decomposition and after 24 h a significant amount of the compound had decomposed. However, interestingly also for this compound type the most abundant signals were still present. Some of the changes in the spectra recorded for **7a** may be due to oxidation of Cys itself (Figure S9). The reactions under the same conditions but with Met are in line with these observations. While **7a** did not react with Met, **1a** slowly decomposed over time (Figures S13 and S14).

A similar set of experiments was conducted for **1a** and **7a** with the DNA model 9-ethylguanine (EtG) by ^{1}H NMR spectroscopy. DNA is considered as the main cellular target of the Ru compound RAED, bearing a bidentate 1,2-ethylenediamine ligand and therefore being structurally related to **1a**. Incubation mixtures at molar ratios of approximately 1:1 and 1:2 (metal complex:EtG) were analyzed 3 and 24 h after mixing by ^{1}H NMR spectroscopy (Figure 6 and Figure S15). Metallacycle **1a** only formed EtG adducts to a minor extent independent of the molar ratio of the incubation mixture, as indicated by the appearance of a signal at around 8.3 ppm which can be assigned to H-8 of Ru-coordinated EtG (Figure S15). After 24 h, the spectra markedly changed and featured several species, again supporting the low stability of **1a**. In contrast, **7a** formed in all cases a defined product with EtG coordinated to the Ru center, while still some

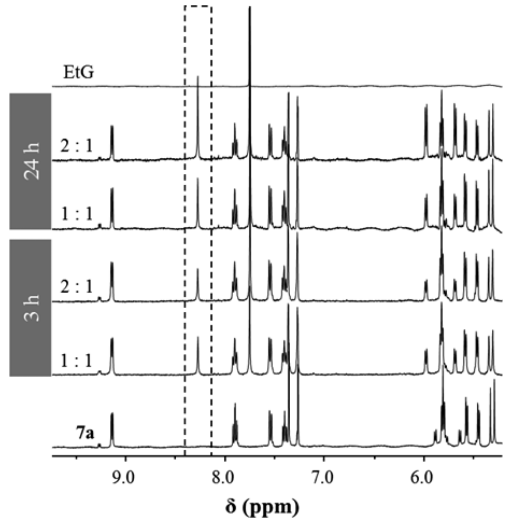

Figure 6. ^{1}H NMR spectroscopic study of the reaction between **7a** and EtG at molar ratios of 1:1 and 1:2 in 10% DMSO-d_6/90% D_2O analyzed after 3 and 24 h. The box indicates the region that features the signal for H-8 of Ru-coordinated EtG.

unreacted EtG was detected (Figure 6). The reaction occurred very quickly, as demonstrated by a significant downfield shift of the H8 signal of EtG from ca. 7.8 to 8.3 ppm, indicating coordination of Ru to N7 of guanine. Integration of the signals at about 8.3 and 9.2 ppm showed after 3 h for both incubation mixtures a ratio of 0.6:1.0 (EtG:**7a**), which changed after 24 h to 1:0.8 and 1:1.3 for the equimolar and 1:2 reaction mixtures, respectively. Addition of another 1 equiv of EtG did not affect the signal at 8.3 ppm but led to an increase in intensity of the peak assigned to H8 of unreacted EtG at ca. 7.8 ppm.

In Vitro Anticancer Activity and Cell Uptake. The in vitro antiproliferative activity of all complexes was studied in HCT116 human colorectal, NCI-H460 non-small-cell lung, SiHa cervical carcinoma, and SW480 colon adenocarcinoma cells. The compounds resulted in a wide range of cytotoxic activity varying from IC_{50} values as low as 6.2 μM to not even reaching the IC_{50} value in the concentration range used (Table 2). In general, the compounds were slightly more active in SiHa cells

Table 2. In Vitro Cytotoxic Activity of Compounds 1a−10a in the Human Cancer Cell Lines HCT116 (Colon), NCI-H460 (Non-Small-Cell Lung), SiHa (Cervix), and SW480 (Colon) As Determined by SRB Assay after 72 h Incubation

	IC_{50} values (μM)			
compound	HCT116	NCI-H460	SiHa	SW480
five-membered				
1a	>250	>250	>250	>250
2a	201 ± 22	174 ± 9	209 ± 13	>215
3a	51 ± 3	48 ± 3	44 ± 1	58 ± 5
4a	16 ± 1	16 ± 0.3	14 ± 1	17 ± 1
5a	>428	>428	>428	>428
6a	199 ± 19	202 ± 23	159 ± 13	223 ± 17
six-membered				
7a	>244	>244	>244	>244
8a	69 ± 15	149 ± 7	57 ± 4	107 ± 11
9a	107 ± 5	130 ± 11	91 ± 3	130 ± 8
10a	8.3 ± 0.6	12 ± 1	6.2 ± 0.02	12 ± 2
RAED-C[a]				5.9 ± 0.7

[a]Taken from ref 53, determined by MTT assay with 96 h incubation.

DOI: 10.1021/acs.organomet.8b00153
Organometallics XXXX, XXX, XXX−XXX

than in the other cell lines tested. Considering the structures of the complexes, the cytotoxicity appeared to be dependent upon the lipophilicity as well as the stability of the complexes. The most lipophilic and stable complexes were potent antiproliferative agents, with IC_{50} values in the low micromolar range (see Table S7 for calculated octanol−water partition coefficients clog*P* for the imidazolium salts as the pro-carbene ligands). Both **4a** and **10a** are based on benzimidazole and feature a benzyl group rather than a methyl group as in their derivatives **2a** and **8a**, and they were the most cytotoxic compounds of the series tested. While the clog*P* value for pro-carbene **4** is higher than that for **10**, the greater stability of **10a** may explain the slightly higher antiproliferative potency. replacing benzimidazole was replaced with imidazole as in **3a** and **9a**, the activity markedly dropped, which was more pronounced in the case of **9a**, for which the antiproliferative activity was 1 order of magnitude lower than that for **10a**. Making the compounds even more hydrophilic by the introduction of ester groups (**5a** and **6a**) caused another decrease in cytotoxicity, with the IC_{50} values increasing significantly. The compound most active in SW480 cells was **10a**, and it showed activity similar to that for the widely studied Ru complex RAED-C, though the conditions used to determine the antiproliferative activity were different.[53]

With the aim of explaining the low antiproliferative activity of **8a** in comparison to **10a**, we determined the cellular accumulation of these complexes in HCT116. The structural difference is that **8a** features a methyl substituent, which in **10a** is replaced with a benzyl group. The cellular content of the complexes was measured through the Ru levels in HCT116 cells after incubations for 4, 24, and 48 h by ICP-MS. Within the first 24 h there was hardly any difference in the intracellular Ru amounts detectable (Figure 7). Incubation experiments for 48 h showed

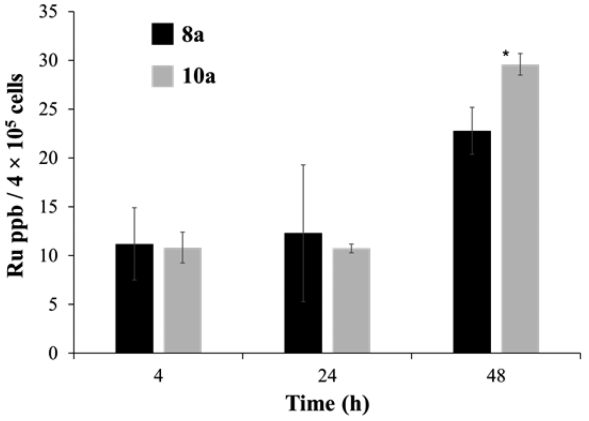

Figure 7. Cellular uptake of compounds **8a** and **10a** in HCT116 cells after incubation for 4, 24, or 48 h. Statistical analysis was carried out using the *t* test (* $p < 0.05$).

that **10a** is taken up into the cells slightly more effectively in comparison to its methyl counterpart **8a** and significantly higher Ru levels for both compounds were measured in comparison to those at the first two time points. Some of the behavior of the complexes may be explained by their lipophilicity (Table S7), which is considerably lower for pro-carbene **8** than for **10**. However, the effect of lipophilicity on cellular uptake was less than expected and cannot fully explain the difference in IC_{50} values between these compounds. The higher cytotoxic activity of **10a** is probably related to additional factors and may be the result of a differing interaction with biological targets due to the hydrophobic benzyl residue.

CONCLUSIONS

Organoruthenium complexes with monodentate NHC ligands have been demonstrated to possess tunable cytotoxic activity depending on the substituents.[21] Herein, we report bidentate NHC-pyridyl ligands and the preparation of the respective Ru(cym) complexes to study the effect of both hydrophobic and hydrophilic groups on their biological activity. The compounds were characterized by standard methods and were found to crystallize as enantiomeric mixtures. In the case of the ester compound **5a**, transesterification was observed in methanol solution.

Stability studies in DMSO with the complexes featuring five (**1a**−**3a**)- or six-membered (**8a** and **10a**) rings as well as the ester-functionalized **5a** and **6a** revealed that **1a** was the least stable compound. In water, **8a** was very stable while **2a** underwent a chlorido/aqua ligand exchange, which was further supported by studies using $AgNO_3$ to abstract the chlorido ligand from the Ru center. We used the five- and six-membered metallacycles **1a** and **7a**, respectively, to investigate the compounds' reactivity with biological molecules. Compound **7a** was stable in the presence of Cys, while **1a** slowly decomposed. This is remarkable, given that many other organoruthenium compounds decompose rapidly in the presence of Cys. In general, both compounds behaved differently; while **7a** reacted with His and EtG, **1a** slowly degraded with His and EtG.

The in vitro anticancer activity studies showed that **10a** was the most active compound in all cell lines investigated, while the more hydrophilic compounds were least active. The effect of the lipophilicity is reflected in the clog*P* values found for the pro-carbenes and taking into consideration the stability of the complexes and therewith the retained +1 charge of the complex cation, while chlorido/aqua exchange would give a +2 charge state. This was confirmed to some extent by the higher cellular accumulation for **10a** in comparison to its closest analogue in the series, **8a**. However, additional factors, such as target interaction, which depends on the substituents, must contribute to the overall biological properties.

EXPERIMENTAL SECTION

General Considerations. All air-sensitive reactions were carried out under an N_2 flow in standard Schlenk or round-bottom flasks. The preparation of Ru^{II}(NHC-pyridin-2-yl) complexes was done in darkness by covering the flask with aluminum foil to prevent photolytic degradation. Solvents such as acetonitrile (MeCN) and dichloromethane (DCM) were dried using a solvent purification system (LC Technology Solutions., SP-1 solvent purifier). Purified solvents were transferred into flasks that were dried under vacuum and purged with N_2 prior to use.

Chemicals and Reagents. The chemicals and solvents were purchased from commercial suppliers. 1-Methylimidazole (99%) was obtained from Arcos Organic, and 2-(bromomethyl)pyridine hydrobromide (98%), imidazole (99%), potassium phosphate tribasic (98%), silver hexafluorophosphate (98%), α-terpinene (89%), and 2-bromopyridine (99%) were purchased from Sigma-Aldrich. Benzimidazole (98%), L-proline (98%), and copper(I) iodide (98%) were obtained from AK Scientific. Ethyl 2-bromoacetate (98%) and iodomethane (99%) were products of Merck. Ruthenium(III) chloride trihydrate (99%) was obtained from Precious Metals Online and silver(I) oxide (AR) from Oakwood Products. Compounds **1**−**10**, **1a**−**3a**, **9a**, and **10a** were synthesized following literature procedures with slight modifications.[39−43]

Physical Measurements. Elemental analyses were conducted on a Vario EL cube (Elementar Analysensysteme GmbH, Hanau, Germany). 1D and 2D ($^1H-^{13}C$ HSQC, and HMBC) NMR spectra were recorded on Bruker Avance AVIII 400 MHz NMR spectrometers at ambient temperature at 400.13 MHz (^1H) or 100.57 MHz ($^{13}C\{^1H\}$). Acetone-d_6, $CDCl_3$, MeOD-d_4, and DMSO-d_6 were used as NMR solvents.

DOI: 10.1021/acs.organomet.8b00153
Organometallics XXXX, XXX, XXX−XXX

High-resolution mass spectra were recorded on a Bruker micrOTOF-Q II ESI-MS instrument in positive ion mode.

X-ray diffraction measurements of single crystals of **4a**–**6a** and **10a** were performed on a Rigaku Oxford Diffraction XtaLAB-Synergy-S single-crystal diffractometer with a PILATUS 200 K hybrid pixel array detector using Cu Kα radiation (λ = 1.54184 Å; Table S2). The X-ray single-crystal diffraction measurement of **8a** was performed on a Siemens/Bruker SMART APEX II single-crystal diffractometer with a CCD area detector using graphite-monochromated Mo Kα radiation (λ = 0.71073 Å). The data were processed with the SHELX2016 and Olex2 software packages.[54,55] All non-hydrogen atoms were refined anisotropically. Hydrogen atoms were inserted at calculated positions and refined with a riding model or without restrictions. Mercury 3.9[56] was used to visualize the molecular structures.

Syntheses. *1-(Pyridin-2-yl)-3-(tert-butylacet-2-yl)imidazolium Bromide (**6**).*

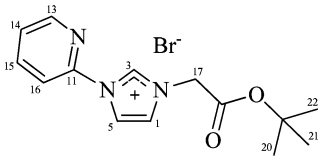

Compound **6** was prepared by refluxing **I** (100 mg, 0.44 mmol) with *tert*-butyl bromoacetate (0.10 mL, 0.63 mmol) in acetonitrile (40 mL) for 24 h. The solvent was removed under reduced pressure, and the crude product was purified by trituration with acetone, affording the pure product as a pale brown solid (0.12 g, 81%). HRMS (ESI$^+$): m/z 260.1389 $[M - Br]^+$ (m_{calc} = 260.1394). ^{1}H NMR (400.13 MHz, DMSO-d_6): δ (ppm) 10.14 (s, 1H, H-3), 8.65–8.68 (m, 1H, H-13), 8.58 (t, ^3J = 2 Hz, 1H, H-5), 8.24 (m, 1H, H-15), 8.08 (d, ^3J = 9 Hz, 1H, H-16), 8.04 (t, ^3J = 2 Hz, 1H, H-1), 7.65–7.69 (m, 1H, H-14), 5.27 (s, 2H, H-17), 1.48 (s, 9H, H-20, H-21, H-22). ^{13}C{^{1}H} NMR (100.57 MHz, DMSO-d_6): δ (ppm) 165.3 (C-18), 149.3 (C-13), 146.43 (C-11), 140.9 (C-15), 136.1 (C-3), 125.5 (C-14), 125.1 (C-1), 119.0 (C-5), 114.5 (C-16), 83.1 (C-19), 50.3(C-17), 27.6 (C-20, C-21, C-22).

General Procedure for the Synthesis of the Ru Complexes. Compounds **1**–**10** (2.0 mol equiv) and silver hexafluorophosphate (2.5–3.0 mol equiv) were added to dry acetonitrile or THF (Table S1) and methanol (1 mL) in a dry Schlenk flask under N_2. The flask was sealed, and the mixture was stirred in darkness at 55 °C for 3 h. Ag_2O (1.4–1.5 mol equiv) was added and the mixture stirred in darkness for a further 24 h at 65 °C. A solution of $[RuCl_2(\eta^6\text{-}p\text{-cymene})]_2$ (1.4–1.5 mol equiv) in dry 1,2-dichloroethane and dichloromethane was added and stirred at 70 °C in darkness overnight. The resultant suspension was filtered over Celite and the filtrate collected and reduced to dryness. Purification was performed via column chromatography over silica ($MeOH/CH_2Cl_2$ 1/25). The solvent of the collected fractions was evaporated, and the crude compound was dissolved in a minimal amount of MeOH and precipitated by addition of diethyl ether. The precipitate was dried in vacuo to afford the Ru(η^6-*p*-cymene) complexes.

*[Chlorido(1-benzyl-3-{pyridin-2-yl}benzimidazol-2-ylidene)(η^6-p-cymene)ruthenium(II)] Hexafluorophosphate (**4a**).*

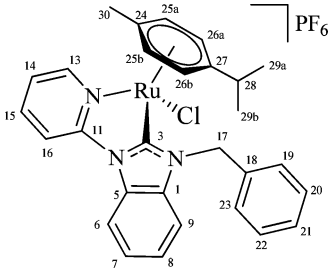

The synthesis of **4a** was performed according to the general procedure using **4** (100 mg, 0.21 mmol), silver hexafluorophosphate (80 mg, 0.32 mmol), silver oxide (48 mg, 0.21 mmol), and $[RuCl_2(\eta^6\text{-}p\text{-cymene})]_2$ (110 mg, 1.7 mol equiv, 0.18 mmol) in dry dichloromethane and 1,2-dichloroethane to afford an orange powder (120 mg, 88%). Single crystals suitable for X-ray diffraction analysis were grown from acetone/diethyl ether. Anal. Calcd for $C_{28}H_{27}ClF_6N_3PRu\cdot0.5H_2O$: C, 48.32; H, 4.05; N, 6.04. Found: C, 48.45; H, 3.94; N, 6.21. HRMS (ESI$^+$): m/z 556.1076 $[M - PF_6]^+$ (m_{calc} = 556.1094). ^{1}H NMR (400.13 MHz, acetone-d_6): δ (ppm) 9.48–9.51 (m, 1H, H-13), 8.61 (d, ^3J = 8 Hz, 1H, H-6), 8.49 (d, ^3J = 8 Hz, 1H, H-16), 8.34 (td, ^3J = 8 Hz, ^4J = 2 Hz, 1H, H-15), 7.54–7.24 (m, 9H, H-7, H-8, H-9, H-19, H-20, H-21, H-22, H-23), 6.42 (dd, ^3J = 7 Hz, ^4J = 1.9 Hz, 1H, H-26a/b), 6.31 (dd, ^3J = 7 Hz, ^4J = 2 Hz, 1H, H-25a/b), 6.21 (d, ^2J = 17 Hz, 1H, H17a/b), 6.16 (dd, ^3J = 7 Hz, ^4J = 2 Hz, 1H, H-25a/b), 5.99 (d, ^2J = 16 Hz, 1H, H17a/b), 5.91 (dd, ^3J = 7 Hz, ^4J = 2 Hz, 1H, H-26a/b), 2.35 (sept, ^3J = 7 Hz, 1H, H-28), 2.11 (s, 3H, H-30), 0.83 (d, ^3J = 7 Hz, 3H, H-29a/b), 0.81 (d, ^3J = 7 Hz, 3H, H-29a/b). ^{13}C{^{1}H} NMR (100.57 MHz, acetone-d_6): δ (ppm) 183.1 (C-3), 156.5 (C-13), 152.6 (C-11), 142.0 (C-15), 135.6 (C-18), 135.2 (C-5), 130.7 (C-1), 129.0 (C-20, C-22), 128.3 (C-21), 127.4 (C-19, C-23), 125.4 (C-8, C-7), 122.9 (C-14), 113.5 (C-16), 113.1 (C-9), 113.0 (C-6), 109.7 (C24), 107.2 (C27), 92.0 (C-25a/b), 88.0 (C-26a/b), 52.8 (C-17), 30.4 (C-24), 22.0 (C-29a/b), 21.8 (C-29a/b), 18.6 (C-30).

*[Chlorido(1-{ethylacet-2-yl}-3-{pyridin-2-yl}imidazol-2-ylidene)-(η^6-p-cymene)ruthenium(II)] Hexafluorophosphate (**5a**).*

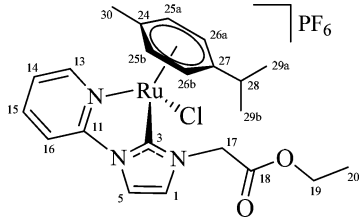

The synthesis of **5a** was performed according to the general procedure using **5** (150 mg, 0.48 mmol), silver hexafluorophosphate (160 mg, 0.65 mmol), silver oxide (75 mg, 0.32 mmol), and $[RuCl_2(\eta^6\text{-}p\text{-cymene})]_2$ (202 mg, 0.33 mmol) in dry acetonitrile to afford a yellow powder (120 mg, 74%). Single crystals suitable for X-ray diffraction analysis were grown from acetone/methanol/diethyl ether. Anal. Calcd for $C_{22}H_{27}ClF_6N_3O_2PRu\cdot H_2O\cdot1.5CH_2Cl_2\cdot0.6MeCN$: C, 36.31; H, 4.17; N, 6.17. Found: C, 36.04; H, 4.00; N, 6.56. HRMS (ESI$^+$): m/z 502.0826 $[M - PF_6]^+$ (m_{calc} = 502.0832). ^{1}H NMR (400.13 MHz, acetone-d_6): δ (ppm) 9.42 (d, ^3J = 6 Hz, 1H, H-13), 8.33 (d, 1H, ^3J = 2 Hz, H-1), 8.30 (t, ^3J = 7 Hz, 1H, H-15), 8.16 (d, ^3J = 8 Hz, 1H, H-16), 7.83 (d, ^3J = 2 Hz, 1H, H-5), 7.57 (t, ^3J = 7 Hz, H, H-14), 6.31 (d, ^3J = 6 Hz, 1H, H-25a/b), 6.22–6.25 (m, 2H, 26a/b, 25a/b), 5.73 (d, ^3J = 6 Hz, 1H, H-25a/b), 5.37–5.48 (m, 2H, 17a/b), 4.39 (quart, ^3J = 7 Hz, 2H, H-19), 2.53 (sept, ^3J = 7 Hz, 1H, H-28), 2.21 (s, 3H, H-30), 1.35 (t, ^3J = 6 Hz, 3H, H-20), 0.98 (d, ^3J = 7 Hz, 6H, H-29a, 29b).^{13}C{^{1}H} NMR (100.57 MHz, acetone-d_6): δ (ppm) 169.4 (C-18), 166.3 (C-3), 156.7 (C-13), 152.9 (C-11), 142.5 (C-15), 127.2 (C-5), 124.2 (C-14), 117.9 (C-1), 113.5 (C-16), 109.3 (C-24), 92.1 (C-25a/b), 91.9 (C-26a/b), 87.8 (C-25a/b), 83.1 (C-26a/b), 63.2 (C-19), 53.1 (C-28), 52.9 (C-17a/b), 31.8 (C-28), 22.7 (C-29a/b), 22.3 (C-29a/b), 19.1 (C-30), 14.4 (C-20a/b).

*[Chlorido(1-{tert-butylacet-2-yl}-3-{pyridin-2-yl}imidazol-2-ylidene)ruthenium(II)] Hexafluorophosphate (**6a**).*

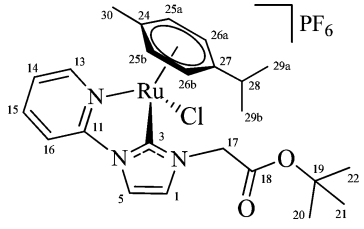

The synthesis of **6a** was performed according to the general procedure using **6** (150 mg, 0.44 mmol), silver hexafluorophosphate (150 mg, 0.58 mmol), silver oxide (100 mg, 1.7 mol equiv, 0.43 mmol), and $[RuCl_2(\eta^6\text{-}p\text{-cymene})]_2$ (180 mg, 0.29 mmol) in dry dichloromethane and 1,2-dichloroethane to afford an orange powder (310 mg, 79%). Anal. Calcd for $C_{24}H_{31}ClF_6N_3O_2PRu\cdot H_2O\cdot2CH_2Cl_2$: C, 36.19; H, 4.32; N, 4.87. Found: C, 36.17; H, 4.26; N, 5.33. HRMS (ESI$^+$): m/z

DOI: 10.1021/acs.organomet.8b00153
Organometallics XXXX, XXX, XXX–XXX

530.1147 $[M - PF_6]^+$ (m_{calc} = 530.1144). ^1H NMR (400.13 MHz, DMSO-d_6): δ (ppm) 9.33 (d, ^3J = 6 Hz, 1H, H-13), 8.48 (d, ^3J = 2 Hz, H-5), 8.29 (td, ^3J = 8 Hz, ^4J = 2 Hz, 1H, H-15), 8.22 (d, ^3J = 8 Hz, 1H, H-14), 7.84 (d, ^3J = 3 Hz, 1H, H-1), 7.56 (td, ^3J = 7 Hz, ^4J = 2 Hz, 1H, H-14), 6.28 (d, ^3J = 7 Hz, 1H, H-25a/b), 6.21 (d, ^3J = 6.4 Hz, 1H, H-26a/b), 6.04 (d, ^3J = 7 Hz, 1H, H-25a/b), 5.75 (d, ^3J = 6 Hz, 1H, H-26a/b), 5.33 (d, ^2J = 17 Hz, 1H, H-17a/b), 5.15 (d, ^2J = 18 Hz, 1H, H-17a/b), 2.68 (sept, ^3J = 7 Hz, 1H, H-28), 2.11 (s, 3H, H-30), 1.55 (s, 9H, H-20a/b/c), 0.86 (d, ^3J = 3 Hz, 3H, H-29a/b), 0.84 (d, ^3J = 3 Hz, 3H, H-29a/b). $^{13}C\{^1H\}$ NMR (100.57 MHz, DMSO-d_6): δ (ppm) 185.6 (C-18), 167.2 (C-3), 155.7 (C-13), 150.8 (C-11), 141.8 (C-15), 126.2 (C-1), 123.1 (C-14), 117.0 (C-5), 115.9 (C-24), 114.7 (C-27), 112.6 (C-16), 90.8 (C-25a/b), 90.6 (C-26a/b), 86.3 (C-26a/b), 83.1 (C-19), 81.8 (C-25a/b), 52.4 (C-17), 30.5 (C-28), 27.7 (C-20a/b/c), 27.6 (C-22a/b), 21.9 (C-29a/b), 18.5 (C-30).

*[Chlorido(1-benzyl-3-{pyridin-2-ylmethyl}imidazol-2-ylidene)(η^6-p-cymene)ruthenium(II)] Hexafluorophosphate (**9a**).*

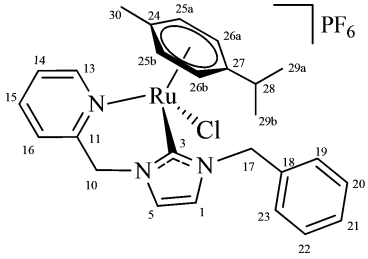

The synthesis of **9a** was performed according to the general procedure using **9** (150 mg, 0.46 mmol), silver hexafluorophosphate (150 mg, 0.60 mmol), silver oxide (75 mg, 0.33 mmol), and $[RuCl_2(\eta^6\text{-}p\text{-cymene})]_2$ (194 mg, 0.32 mmol) in dry dichloromethane and 1,2-dichloroethane to afford an orange powder (70 mg, 46%). Anal. Calcd for $C_{26}H_{29}ClF_6N_3PRu{\cdot}0.2CH_3(CH_2)_4CH_3$: C, 47.88; H, 4.70; N, 6.16. Found: C, 47.57; H, 4.34; N, 5.85. HRMS (ESI^+): m/z 520.1075 $[M - PF_6]^+$ (m_{calc} = 520.1092). ^1H NMR (400.13 MHz, DMSO-d_6): δ (ppm) 9.22 (d, ^3J = 6 Hz, 1H, H-13), 8.08 (td, ^3J = 8 Hz, ^4J = 2 Hz, 1H, H-15), 7.71 (d, ^3J = 8 Hz, 1H, H-16), 7.66 (d, ^3J = 8 Hz, 1H, H-1) 7.56 (t, ^3J = 7 Hz, 1H, H-5), 7.34–7.45 (m, 5H, H-19, H-23, H-21, H-22, H-20), 7.24 (d, ^3J = 8 Hz, 1H, H-1), 5.87 (d, ^3J = 6 Hz, 1H, H-26a/b), 5.82, (dd, ^3J = 17 Hz, ^4J = 6 Hz, 1H, H-25a/b), 5.66 (d, ^3J = 16 Hz, 1H, H-10a/b), 5.56–5.63 (m, 2H, H-23, H26a/b), 5.44 (d, ^3J = 15 Hz, 2H, H-17a/b), 4.98 (d, ^3J = 16 Hz, 1H, H-10a/b), 2.69–2.77 (m, 1H, H-28), 2.06 (s, 3H, C30), 1.10 (d, ^3J = 7 Hz, 6H, H-29a, H-29b). $^{13}C\{^1H\}$ NMR (100.57 MHz, acetone-d_6): δ (ppm) 176.2 (C-11), 159.9 (C-13), 157.5 (C-3), 140.6 (C-15), 137.7 (C-18), 129.7 (C- 23/19), 129.4 (C-22/20), 129.1 (C-21), 125.9 (C-1), 125.6 (C-5), 123.9 (C-16), 123.6 (C-14), 112.4 (C-27), 103.3 (C-24), 90.1 (C-25a/b), 87.2 (C-26a/b), 85.7 (C-25a/b), 85.6 (C-26a/b), 55.0 (C-710a/b), 54.5 (C-17), 32.3 (C-28), 24.0 (C-30), 21.4 (C-29a/b), 18.7 (C-29a/b).

*[Chlorido(1-benzyl-3-{pyridin-2-ylmethyl}benzimidazol-2-ylidene)(η^6-p-cymene)ruthenium(II)] Hexafluorophosphate (**10a**).*

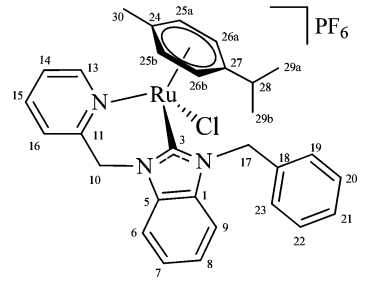

The synthesis of **10a** was performed according to the general procedure using **10** (150 mg, 0.40 mmol), silver hexafluorophosphate (130 mg, 0.51 mmol), silver oxide (90 mg, 1.96 mol equiv, 0.39 mmol), and $[RuCl_2(\eta^6\text{-}p\text{-cymene})]_2$ (180 mg, 0.30 mmol) in dry dichloromethane and 1,2-dichloroethane to afford an orange powder (75 mg, 42%). Single crystals suitable for X-ray diffraction analysis were grown from acetone/diethyl ether. Anal. Calcd for $C_{30}H_{31}ClF_6N_3PRu{\cdot}0.3H_2O$: C, 50.01; H, 4.42; N, 5.83. Found: C, 50.28; H, 4.79; N, 5.72. HRMS (ESI^+): m/z 570.1267 $[M - PF_6]^+$ (m_{calc} = 570.1245). ^1H NMR (400.13 MHz, DMSO-d_6): δ (ppm) 9.25 (d, ^3J = 6 Hz, 1H, H-13), 8.13 (td, ^3J = 8 Hz, ^4J = 2 Hz, 1H, H-15), 8.08 (d, ^3J = 8.4 Hz, 1H, H-6), 7.96 (dd, ^3J = 8 Hz, ^4J = 2 Hz, 1H, H- 16), 7.61 (td, ^3J = 7 Hz, ^4J = 2 Hz, 1H, H-14), 7.44–7.42 (m, 8H, H-19, H-21, H-23, H-20, H-22, H-7, H-8, H-9), 6.27 (d, ^2J = 17 Hz, 1H, H-10a/b), 5.96 (dd, ^3J = 6 Hz, ^4J = 2 Hz, 1H, H-26a/b), 5.93 (s, 2H, H-17), 5.82 (dd, ^3J = 6 Hz, ^4J = 2 Hz, 1H, H-25a/b), 5.77 (dd, ^3J = 6 Hz, ^4J = 2 Hz, 1H, H-25a/b), 5.67 (dd, ^3J = 7 Hz, ^4J = 2 Hz, 1H, H-26a/b), 5.08 (d, ^2J = 16 Hz, 1H, H-10a/b), 2.73 (sept, ^3J = 7 Hz, 1H, H-27), 2.02 (s, 3H, H-30), 1.13 (d, ^3J = 7 Hz, 3H, H-29a/b), 1.05 (d, ^3J = 7 Hz, 3H, H-29a/b). $^{13}C\{^1H\}$ NMR (100.57 MHz, DMSO-d_6): δ (ppm) 190.7 (C-11), 156.5 (C-13), 151.7 (C-3), 139.9 (C-15), 136.4 (C-18), 134.2 (C-5), 133.8 (C-1), 128.7 (C- 19/23), 127.8 (C-21), 126.5 (C-20/22), 125.1 (C-7), 124.7 (C-8/14),123.5 (C-8/14), 111.7 (C-6), 111.1 (C-27), 110.6 (C-9), 101.45 (C-24), 88.8 (C-25a/b), 87.8 (C-26a/b), 85.8 (C-25a/b), 85.2 (C-26a/b), 51.4 (C-10a/b), 49.7 (C-17), 30.7 (C-28), 22.7 (C-30), 21.1 (C-29a/b), 17.9 (C-29a/b).

Stability Studies. For the stability studies in DMSO, **1a**–**3a**, **5a**, **6a**, **8a**, and **10a** (1–2 mg) were dissolved in in DMSO-d_6 and ^1H NMR spectra were recorded after 0, 1, 3, 12, 24, 48, and 72 h. To determine their stability in aqueous solution, **2a** and **8a** (1–2 mg) were dissolved in DMSO-d_6 and diluted with D_2O (1/5) and ^1H NMR spectra were collected over 3 days. The same experiment was conducted but with 1 equiv of $AgNO_3$ added to induce the exchange of the chlorido with an aqua ligand.

DFT Calculations. GAUSSIAN 09W[57] was used to calculate the optimized ground-state structures and frequencies for the different molecules by density functional theory (DFT) with the B3LYP hybrid exchange functional and a split basis set for C, H, N, O, and Cl (6-31G(d,p)) and the transition metal ruthenium (SDDAll) under vacuum. The SCRF (self-consistent reaction field) keyword was implemented for the optimization of aqueous simulation of the molecules. This method is the integral equation formalism variant of the polarizable continuum model (IEFPCM).[58] The frontier orbitals were viewed and obtained through the Avogadro software (version 1.2.0).[59]

Biomolecule Interactions. The biomolecule interactions of **1a** and **7a** were studied by ^1H NMR spectroscopy. Complexes **1a** and **7a** were dissolved in DMSO-d_6 and diluted with D_2O to obtain a 20% DMSO-d_6/80% D_2O solution. Equimolar amounts of the amino acids Met, Cys, and His were added to each complex, and ^1H NMR spectra were collected over periods of up to 24 h. The ^1H NMR spectra for the reactions of each complex and 9-ethylguanine at equimolar and 1:2 ratios were recorded 3 and 24 h after mixing.

Sulforhodamine B Cytotoxicity Assay. HCT116, SW480, and NCI-H460 cells were supplied by ATCC, while SiHa cells were obtained from Dr. David Cowan, Ontario Cancer Institute, Canada. The cells were grown in αMEM (Life Technologies) supplemented with 5% fetal calf serum (Moregate Biotech) at 37 °C in a humidified incubator with 5% CO_2.

The cells were seeded at 750 (HCT116, NCI-H460), 4000 (SiHa), or 5000 (SW480) cells/well in 96-well plates and left to settle for 24 h. The compounds were added to the plates in a series of 3-fold dilutions, containing a maximum of 0.5% DMSO at the highest concentration. The assay was terminated after 72 h by addition of 10% trichloroacetic acid (Merck Millipore) at 4 °C for 1 h. The cells were stained with 0.4% sulforhodamine B (Sigma-Aldrich) in 1% acetic acid for 30 min in the dark at room temperature and then washed with 1% acetic acid to remove unbound dye. The stain was dissolved in unbuffered Tris base (10 mM; Serva) for 30 min on a plate shaker in the dark and quantified on a BioTek EL808 microplate reader at an absorbance wavelength of 490 nm with 450 nm as the reference wavelength to determine the percentage of cell growth inhibition by determining the absorbance of each sample relative to a negative (no inhibitor) and a no-growth control (day 0). The IC_{50} values were calculated with SigmaPlot 12.5 using a three-parameter logistic sigmoidal dose–response curve between the calculated growth inhibition and the compound concentration. The presented IC_{50} values are the mean of at least 3 independent experiments, where 10 concentrations were tested in duplicate for each compound.

DOI: 10.1021/acs.organomet.8b00153
Organometallics XXXX, XXX, XXX–XXX

Cellular Accumulation. The cellular uptake experiments were carried out as described previously. HCT116 cells (4×10^5 /well) were seeded into 6-well plates and allowed to settle for 24 h at 37 °C and 5% CO_2. Compounds **8a** and **10a** were dissolved in DMSO (6900 and 824 μM, respectively) and diluted with media to a concentration of 1% DMSO to reach their previously determined IC_{50} values. The cells were incubated with metal complexes for 4, 24, and 48 h, after which the medium was removed and the cells were washed twice with 1 mL of ice-cold PBS buffer. The cells were lysed with 2 mL of concentrated nitric acid (containing 0.1 μL of a 1000 ± 3 μg/mL thulium standard as internal standard) and digested with an Ethos Up microwave digestion system (Milestone). After the solutions were diluted with 10 mL of H_2O, the ruthenium content was determined by ICP-MS (Agilent 7700) with an ASX-500 autosampler (CETAC Technologies) in a Serie SuSi laminar flow hood (SPECTEC) equipped with a MicroMist nebulizer and a Scott double-pass spray chamber. The carrier gas flow rate was 1 mL min^{-1}. The instrument was tuned for cerium, cobalt, lithium, magnesium, thallium, and yttrium. The reported values are the mean of at least three independent uptake experiments conducted with blank wells for each substance to account for unspecific binding to the plastic of the well plates.

■ ASSOCIATED CONTENT

Supporting Information

The Supporting Information is available free of charge on the ACS Publications website at DOI: 10.1021/acs.organomet.8b00153.

Preparation and characterization of all organic and organometallic compounds not given in the Experimental Section, X-ray crystallographic data, and additional figures, as well as time-dependent NMR spectra recorded for the stability studies and biomolecule interaction experiments (PDF)

Accession Codes

CCDC 1826988−1826992 contain the supplementary crystallographic data for this paper. These data can be obtained free of charge via www.ccdc.cam.ac.uk/data_request/cif, or by emailing data_request@ccdc.cam.ac.uk, or by contacting The Cambridge Crystallographic Data Centre, 12 Union Road, Cambridge CB2 1EZ, UK; fax: +44 1223 336033.

■ AUTHOR INFORMATION

Corresponding Author

* C.G.H.: e-mail, c.hartinger@auckland.ac.nz; web, http://hartinger.auckland.ac.nz; tel, +64 9 3737 599 ext 83220.

ORCID

Muhammad Hanif: 0000-0002-2256-2317

Christian G. Hartinger: 0000-0001-9806-0893

Notes

The authors declare no competing financial interest.

■ ACKNOWLEDGMENTS

We thank the University of Auckland (University of Auckland Doctoral Scholarship to H.U.H. and K.K.H.T.) for financial support. We are grateful to Tanya Groutso for collecting the single-crystal X-ray diffraction data and Tony Chen for ESI-MS analyses.

■ REFERENCES

(1) Peris, E. *Chem. Rev.* **2017**, DOI: 10.1021/acs.chemrev.6b00695.

(2) Janssen-Muller, D.; Schlepphorst, C.; Glorius, F. *Chem. Soc. Rev.* **2017**, *46*, 4845−4854.

(3) Nasr, A.; Winkler, A.; Tamm, M. *Coord. Chem. Rev.* **2016**, *316*, 68−124.

(4) Johnson, C.; Albrecht, M. *Coord. Chem. Rev.* **2017**, *352*, 1−14.

(5) Charra, V.; de Fremont, P.; Braunstein, P. *Coord. Chem. Rev.* **2017**, *341*, 53−176.

(6) Farrell, J. M.; Posaratnanathan, R. T.; Stephan, D. W. *Chem. Sci.* **2015**, *6*, 2010−2015.

(7) Nair, A. G.; McBurney, R. T.; Walker, D. B.; Page, M. J.; Gatus, M. R. D.; Bhadbhade, M.; Messerle, B. A. *Dalton Trans.* **2016**, *45*, 14335−14342.

(8) Herrmann, W. A. *Angew. Chem., Int. Ed.* **2002**, *41*, 1290−1309.

(9) Viciu, M. S.; Germaneau, R. F.; Navarro-Fernandez, O.; Stevens, E. D.; Nolan, S. P. *Organometallics* **2002**, *21*, 5470−5472.

(10) Ruiz-Castillo, P.; Buchwald, S. L. *Chem. Rev.* **2016**, *116*, 12564−12649.

(11) Poyatos, M.; Uriz, P.; Mata, J. A.; Claver, C.; Fernandez, E.; Peris, E. *Organometallics* **2003**, *22*, 440−444.

(12) Do, J. L.; Mottillo, C.; Tan, D.; Strukil, V.; Friscic, T. *J. Am. Chem. Soc.* **2015**, *137*, 2476−2479.

(13) Kantchev, E. A. B.; O'Brien, C. J.; Organ, M. G. *Angew. Chem., Int. Ed.* **2007**, *46*, 2768−2813.

(14) Bernet, L.; Lalrempuia, R.; Ghattas, W.; Mueller-Bunz, H.; Vigara, L.; Llobet, A.; Albrecht, M. *Chem. Commun.* **2011**, *47*, 8058−8060.

(15) Leigh, V.; Ghattas, W.; Lalrempuia, R.; Muller-Bunz, H.; Pryce, M. T.; Albrecht, M. *Inorg. Chem.* **2013**, *52*, 5395−5402.

(16) Liu, W. K.; Gust, R. *Chem. Soc. Rev.* **2013**, *42*, 755−773.

(17) Chan, C. Y.; Barnard, P. J. *Dalton Trans.* **2015**, *44*, 19126−19140.

(18) Medici, S.; Peana, M.; Crisponi, G.; Nurchi, V. M.; Lachowicz, J. I.; Remelli, M.; Zoroddu, M. A. *Coord. Chem. Rev.* **2016**, *327-328*, 349−359.

(19) Liu, W. K.; Gust, R. *Coord. Chem. Rev.* **2016**, *329*, 191−213.

(20) Cetinkaya, B.; Cetinkaya, E.; Kucukbay, H.; Durmaz, R. *Arzneim.-Forsch.* **1996**, *46*, 821−823.

(21) Oehninger, L.; Rubbiani, R.; Ott, I. *Dalton Trans.* **2013**, *42*, 3269−3284.

(22) Oehninger, L.; Stefanopoulou, M.; Alborzinia, H.; Schur, J.; Ludewig, S.; Namikawa, K.; Munoz-Castro, A.; Koster, R. W.; Baumann, K.; Wolfl, S.; Sheldrick, W. S.; Ott, I. *Dalton Trans.* **2013**, *42*, 1657−1666.

(23) Melaiye, A.; Simons, R. S.; Milsted, A.; Pingitore, F.; Wesdemiotis, C.; Tessier, C. A.; Youngs, W. J. *J. Med. Chem.* **2004**, *47*, 973−977.

(24) Berners-Price, S. J.; Filipovska, A. *Metallomics* **2011**, *3*, 863−873.

(25) Hickey, J. L.; Ruhayel, R. A.; Barnard, P. J.; Baker, M. V.; Berners-Price, S. J.; Filipovska, A. *J. Am. Chem. Soc.* **2008**, *130*, 12570−1.

(26) Pellei, M.; Gandin, V.; Marinelli, M.; Orsetti, A.; Del Bello, F.; Santini, C.; Marzano, C. *Dalton Trans.* **2015**, *44*, 21041−21052.

(27) Hartinger, C. G.; Dyson, P. J. *Chem. Soc. Rev.* **2009**, *38*, 391−401.

(28) Murray, B. S.; Babak, M. V.; Hartinger, C. G.; Dyson, P. J. *Coord. Chem. Rev.* **2016**, *306*, 86−114.

(29) Zhang, P.; Sadler, P. J. *J. Organomet. Chem.* **2017**, *839*, 5−14.

(30) Thota, S.; Rodrigues, D. A.; Crans, D. C.; Barreiro, E. J. *J. Med. Chem.* **2018**, DOI: 10.1021/acs.jmedchem.7b01689.

(31) Meier-Menches, S. M.; Gerner, C.; Berger, W.; Hartinger, C. G.; Keppler, B. K. *Chem. Soc. Rev.* **2018**, *47*, 909−928.

(32) Hanif, M.; Nazarov, A. A.; Legin, A.; Groessl, M.; Arion, V. B.; Jakupec, M. A.; Tsybin, Y. O.; Dyson, P. J.; Keppler, B. K.; Hartinger, C. G. *Chem. Commun.* **2012**, *48*, 1475−1477.

(33) Adhireksan, Z.; Davey, G. E.; Campomanes, P.; Groessl, M.; Clavel, C. M.; Yu, H.; Nazarov, A. A.; Yeo, C. H. F.; Ang, W. H.; Dröge, P.; Rothlisberger, U.; Dyson, P. J.; Davey, C. A. *Nat. Commun.* **2014**, *5*, 3462.

(34) Soldevila-Barreda, J. J.; Romero-Canelón, I.; Habtemariam, A.; Sadler, P. J. *Nat. Commun.* **2015**, *6*, 6582.

(35) Kubanik, M.; Holtkamp, H.; Söhnel, T.; Jamieson, S. M. F.; Hartinger, C. G. *Organometallics* **2015**, *34*, 5658−5668.

DOI: 10.1021/acs.organomet.8b00153
Organometallics XXXX, XXX, XXX−XXX

(36) Aman, F.; Hanif, M.; Kubanik, M.; Ashraf, A.; Söhnel, T.; Jamieson, S. M. F.; Siddiqui, W. A.; Hartinger, C. G. *Chem. - Eur. J.* **2017**, *23*, 4893−4902.
(37) Kubanik, M.; Lam, N. Y. S.; Holtkamp, H. U.; Sohnel, T.; Anderson, R. F.; Jamieson, S. M. F.; Hartinger, C. G. *Chem. Commun.* **2018**, *54*, 992−995.
(38) Xi, Z. X.; Liu, F. H.; Zhou, Y. B.; Chen, W. Z. *Tetrahedron* **2008**, *64*, 4254−4259.
(39) Jahnke, M. C.; Pape, T.; Hahn, F. E. *Eur. J. Inorg. Chem.* **2009**, *2009*, 1960−1969.
(40) Lv, R.; Wang, Y. X.; Zhou, C. S.; Li, L. Y.; Wang, R. H. *ChemCatChem* **2013**, *5*, 2978−2982.
(41) Barbante, G. J.; Francis, P. S.; Hogan, C. F.; Kheradmand, P. R.; Wilson, D. J. D.; Barnard, P. J. *Inorg. Chem.* **2013**, *52*, 7448−7459.
(42) Chan, C. Y.; Pellegrini, P. A.; Greguric, I.; Barnard, P. J. *Inorg. Chem.* **2014**, *53*, 10862−10873.
(43) Barbante, G. J.; Doeven, E. H.; Francis, P. S.; Stringer, B. D.; Hogan, C. F.; Kheradmand, P. R.; Wilson, D. J. D.; Barnard, P. J. *Dalton Trans.* **2015**, *44*, 8564−8576.
(44) Grundemann, S.; Kovacevic, A.; Albrecht, M.; Faller, J. W.; Crabtree, R. H. *J. Am. Chem. Soc.* **2002**, *124*, 10473−10481.
(45) Chiu, P. L.; Lai, C. L.; Chang, C. F.; Hu, C. H.; Lee, H. M. *Organometallics* **2005**, *24*, 6169−6178.
(46) Oehninger, L.; Stefanopoulou, M.; Alborzinia, H.; Schur, J.; Ludewig, S.; Namikawa, K.; Muñoz-Castro, A.; Köster, R. W.; Baumann, K.; Wölfl, S. *Dalton Trans.* **2013**, *42*, 1657−1666.
(47) Fernandez, F. E.; Puerta, M. C.; Valerga, P. *Organometallics* **2012**, *31*, 6868−6879.
(48) Tay, B. Y.; Wang, C.; Phua, P. H.; Stubbs, L. P.; Huynh, H. V. *Dalton Trans.* **2016**, *45*, 3558−63.
(49) Viji, M.; Tyagi, N.; Naithani, N.; Ramaiah, D. *New J. Chem.* **2017**, *41*, 12736−12745.
(50) Kandioller, W.; Kurzwernhart, A.; Hanif, M.; Meier, S. M.; Henke, H.; Keppler, B. K.; Hartinger, C. G. *J. Organomet. Chem.* **2011**, *696*, 999−1010.
(51) Hanif, M.; Meier, S. M.; Adhireksan, Z.; Henke, H.; Martic, S.; Movassaghi, S.; Labib, M.; Kandioller, W.; Jamieson, S. M. F.; Hejl, M.; Jakupec, M. A.; Kraatz, H. B.; Davey, C. A.; Keppler, B. K.; Hartinger, C. G. *ChemPlusChem* **2017**, *82*, 841−847.
(52) Movassaghi, S.; Hanif, M.; Holtkamp, H. U.; Söhnel, T.; Jamieson, S. M. F.; Hartinger, C. G. *Dalton Trans.* **2018**, *47*, 2192−2201.
(53) Babak, M. V.; Meier, S. M.; Legin, A. A.; Razavi, M. S. A.; Roller, A.; Jakupec, M. A.; Keppler, B. K.; Hartinger, C. G. *Chem. - Eur. J.* **2013**, *19*, 4308−4318.
(54) Dolomanov, O. V.; Bourhis, L. J.; Gildea, R. J.; Howard, J. A. K.; Puschmann, H. *J. Appl. Crystallogr.* **2009**, *42*, 339−341.
(55) Sheldrick, G. M. *Acta Crystallogr., Sect. C: Struct. Chem.* **2015**, *71*, 3−8.
(56) Macrae, C. F.; Edgington, P. R.; McCabe, P.; Pidcock, E.; Shields, G. P.; Taylor, R.; Towler, M.; van de Streek, J. *J. Appl. Crystallogr.* **2006**, *39*, 453−457.
(57) Frisch, M.; Trucks, G.; Schlegel, H. B.; Scuseria, G.; Robb, M.; Cheeseman, J.; Scalmani, G.; Barone, V.; Mennucci, B., et al. *Gaussian 09W*; Gaussian, Inc., Wallingford, CT, 2009.
(58) Scalmani, G.; Frisch, M. J. *J. Chem. Phys.* **2010**, *132*, 114110.
(59) Hanwell, M. D.; Curtis, D. E.; Lonie, D. C.; Vandermeersch, T.; Zurek, E.; Hutchison, G. R. *J. Cheminf.* **2012**, *4*, 17.

DOI: 10.1021/acs.organomet.8b00153
Organometallics XXXX, XXX, XXX−XXX